Front. Mater. Sci. 2023, 17(1): 230638
https://doi.org/10.1007/s11706-023-0638-8

RESEARCH ARTICLE

Double-layered TiO_2 cavity/nanoparticle photoelectrodes for efficient dye-sensitized solar cells

Zhen Li[1,2] and Libo Yu (✉)[1,2]

1 College of Chemistry and Chemical Engineering, Hexi University, Zhangye 734000, China
2 Key Laboratory of Hexi Corridor Resources Utilization of Gansu, Hexi University, Zhangye 734000, China

ABSTRACT: **TiO_2 nanoparticles (NPs) in the size of ~25 nm, namely P25, are very common material as the electron collecting layer in dye-sensitized solar cells (DSSCs). However, the light-scattering improvement of TiO_2 NP photoelectrodes is still a challenge. Here, we built TiO_2 cavities on the top of the TiO_2 NP layer by using carbonaceous microspheres as the template, forming the TiO_2 cavity/nanoparticle (C/NP) photoelectrode for the application in DSSCs. The cavity amount in the TiO_2 C/NP photoelectrode was controlled by adjusting the weight ratio of carbonaceous microspheres. SEM results confirm the successful formation of the double-layered TiO_2 C/NP electrode. *J*–*V* tests show that the optimized TiO_2 C/NP electrode prepared with 25 wt.% carbonaceous microspheres contributes to remarkable improvement of the short-circuit current density (J_{sc}) and the power conversion efficiency (PCE). The best photovoltaic performance solar cell with the PCE of 9.08% is achieved with the optimized TiO_2 C/NP photoelectrode, which is over 98% higher than that of the TiO_2 NP photoelectrode. Further investigations of UV-vis DRS, IPCE, OCVD, and EIS demonstrate that the competition between light scattering effect and charges recombination in this TiO_2 C/NP photoelectrode is responsible for the PCE enhancement.**

KEYWORDS: **titanium dioxide; dye sensitized solar cell; cavity; light scattering**

Contents

Received August 22, 2022; accepted January 8, 2023

E-mail: yulibo_665@163.com

1 Introduction

As one of the most competitive types of the third-generation solar cells, dye-sensitized solar cells (DSSCs) have become a hotspot in the field of solar cell research due to their several advantages including the easy fabrication process, the use of nontoxic materials, and the designability of flexible devices [1–2]. DSSCs are

typically assembled with three parts, including organic dye-sensitized electron transport layer built by TiO_2 nanoparticles (NPs) in the size of ~25 nm (known as P25) film as the photoelectrode, I^-/I_3^- solution as the redox electrolyte, and Pt-coated fluorine-doped tin oxide (FTO) glass as the counter electrode [3]. So far, investigators have done much research work to optimize the photovoltaic performance of DSSCs, such as synthesizing efficient organic dyes [4–5], designing new microstructures of TiO_2 [6–7], and developing low-price counter electrode materials to replace the conventional expensive Pt [8–9]. As is well known, the TiO_2 NP photoelectrodes are most widely used in DSSCs because of their high specific area for the dye adsorption [10–11]. However, the TiO_2 NP photoelectrodes always experience bad light scattering because of small NPs and 5–15 nm pores in the TiO_2 NP layer [12]. A strategy building the light-scattering center or layer could be a solution to overcome this drawback [13].

Generally, two approaches could be performed to generate light-scattering effects in the photoelectrode. One is the construction of large-size TiO_2 structures, such as TiO_2 beads [14–16], microspheres [17–19], hollow microspheres [20–22], nanotubes [23–24], and nanorods [25–26]. Another approach could be the building of TiO_2 cavities in the photoelectrode. Microsphere templates such as polystyrene spheres or carbon spheres are suitable candidates to create cavities in the photoelectrode [27]. During the sintering process, such templates embedded in the TiO_2 NP photoelectrode would be sacrificed, leaving cavities which function as light-scattering centers in the photoelectrode [12,28]. Nevertheless, cavities in the TiO_2 NP photoelectrode may destroy the mesoporous scaffold and prolong the pathway of electrons. Meanwhile, building cavities in the TiO_2 NP photoelectrode is still an attractive strategy because of its low synthesis cost and easy fabrication process.

In this study, we prepared carbonaceous microspheres in the size of ~500 nm and used them as the template to make the TiO_2 cavity layer on the top of the TiO_2 NP photoelectrode prepared by P25, forming the TiO_2 cavity/nanoparticle (C/NP) photoelectrode. The weight ratio of carbonaceous microspheres was set in the range of 0–50 wt.% to build double-layered TiO_2 NP and TiO_2 C/NP photoelectrodes with a controlled amount of cavities. Based on such photoelectrodes, DSSCs were assembled and their photovoltaic performance was measured. The best power conversion efficiency (PCE) of 9.08% was obtained with an optimized TiO_2 C/NP photoelectrode, which is over 98% higher than that of the TiO_2 NP photoelectrode. Further investigations demonstrated that the increase in the photovoltaic performance of this optimized TiO_2 C/NP-based DSSC can be attributed to the competition between light scattering effect and charges recombination in the TiO_2 C/NP photoelectrode.

2 Experimental

2.1 Materials

Analytical pure chemical reagent, including sucrose, ethylcellulose, terpineol, and ethanol, were ordered from Aladdin Co., Ltd. (Shanghai, China). These chemicals were used directly without further purification. Other materials such as commercial P25, conductive FTO glass, organic dye di-tetrabutylammonium *cis*-bis(isothiocyanato)-bis(2,2′-bipyridyl-4,4′-dicarboxylato)-ruthenium(II) (abbreviated as N719), Pt/FTO counter electrode, and I^-/I_3^- electrolyte were offered by Opvtech Co., Ltd. (Dalian, China).

2.2 Building of TiO_2 NP layer on FTO

The slurry composed of 0.2 g ethylcellulose, 3 mL terpineol, 2 mL ethanol, and 1.0 g P25 was spin-coated on the conductive surface of the FTO glass which was cut in advance into the size of 2.0 cm × 1.5 cm. Then the product was transferred into a Muffle furnace and sintered at 450 °C for 30 min to burn out organic residues, and finally the TiO_2 NP electrode was produced.

2.3 Formation of TiO_2 cavities on the top of TiO_2 NP layer

Carbonaceous microspheres were firstly synthesized as the hard template according to Ref. [29] for making cavities in TiO_2 NPs. Briefly, the 1.5 $mol \cdot L^{-1}$ sucrose aqueous solution was added into 100 mL stainless autoclave with 80% volume and sealed. Subsequently, the stainless autoclave was put into an electric oven to complete the hydrothermal reaction. The hydrothermal reaction condition was set to 160 °C for 8 h.

Carbonaceous microspheres, P25, ethylcellulose (0.2 g), terpineol (3 mL), and ethanol (2 mL) were mixed together to get a homogenous viscous mixture. Then, the viscous

mixture was doctor-bladed on the top of the prepared TiO_2 NP electrode. After dried in air, the product was sintered again in the Muffle furnace at 450 °C for 1 h to burn out carbonaceous microspheres, leaving cavities inside the top layer of the TiO_2 NP electrode. The resultant photoelectrode is hereafter abbreviated as TiO_2 C/NP. The amount of cavities in TiO_2 C/NP is tuned by the weight ratio of carbonaceous microspheres in the mixture. We prepared TiO_2 C/NP with the weight ratio of carbonaceous microspheres in 12.5, 25, and 37.5 wt.%, which are abbreviated as TiO_2 C/NP (12.5 wt.%), TiO_2 C/NP (25 wt.%), and TiO_2 C/NP (37.5 wt.%), respectively. A double-layered TiO_2 NP photoelectrode was also prepared as a comparative study.

2.4 Dye sensitization and solar cell assembly

The 0.3 $mmol \cdot L^{-1}$ N719 ethanol solution was used to complete the dye loading on the photoelectrode. Specifically, the series of TiO_2 C/NP electrodes and the TiO_2 NP electrode were dipped into the N719 solution for 72 h at room temperature. Then, these photoelectrodes were rinsed with ethanol and dried in air.

The DSSC was assembled in an open way like a sandwich by inserting the I^-/I_3^- electrolyte between the dye-sensitized photoelectrode and the Pt/FTO counter electrode [30].

2.5 Characterization

The morphology and the structure of carbonaceous microspheres and photoelectrodes (i.e., TiO_2 NP and TiO_2 C/NP) were characterized by field-emission scanning electron microscopy (FE-SEM, FEI-Quanta 250) and transmission electron microscopy (TEM, FEI Tecnai G2). A Quantachrome NOVA 4200e system was used to test nitrogen adsorption–desorption isotherms. Before the test, samples were degassed at 250 °C for 12 h under vacuum. Based on nitrogen adsorption–desorption isotherms, the specific surface areas of TiO_2 C/NP photoelectrodes were calculated according to the Brunar–Emmett–Teller (BET) method. The diffuse reflectance spectroscopy (DRS) results of those photoelectrodes were obtained by an ultraviolet-visible (UV-vis) spectrophotometer (Hitachi U4100).

J–V behaviors of the DSSCs were analyzed by a Keithley 2400 source meter under AM 1.5 simulated sunlight with a power density of 100 $mW \cdot cm^{-2}$. The measurements of the incident photon-to-current conversion efficiency (IPCE) spectrum were conducted by the 150 W Xe lamp coupled with a computer-controlled monochromator. The open-circuit voltage decay (OCVD) measurement and the electrochemical impedance spectroscopy (EIS) were carried out on the electrochemical workstation CHI 660E. The DSSCs for the OCVD tests were illuminated under AM 1.5 simulated sunlight, and the variation of voltage with time was recorded after turning off the simulated sunlight. The EIS was performed under dark at a bias of −0.72 V with the frequency range from 0.1 to 10^5 Hz.

3 Results and discussion

The carbonaceous microspheres play the role of template to make cavities in the TiO_2 NP photoelectrode. Figure 1(a) shows the SEM image of carbonaceous microspheres prepared by the hydrothermal method using the sucrose aqueous solution as the raw material. Apparently, microspheres with the size around 500 nm are successfully obtained. The TEM image of carbonaceous microspheres is also presented in Fig. 1(b), indicating that the products are solid spheres with the size around 500 nm.

Figure S1(a) provides the top surface morphology of the TiO_2 NP photoelectrode (see ESI). It can be seen that the surface is distributed with uniform size of ~25 nm TiO_2 NPs, and only small pores around 30 nm exist among NPs. The cross-section view is presented in Fig. S1(b), showing that the thickness of the TiO_2 NP photoelectrode is about 15 μm with a double-layered structure. Both the top surface and the cross-section SEM images display the homogenous distribution of NPs, indicating a dense TiO_2 NP scaffold film formed on the FTO glass.

When the TiO_2 cavity layer was formed using

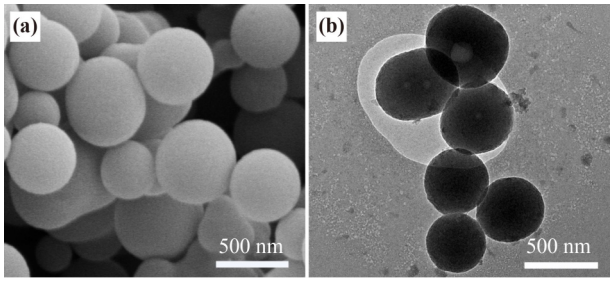

Fig. 1 Morphology of carbonaceous microspheres: (**a**) SEM image; (**b**) TEM image.

carbonaceous microspheres as the template, the surface morphology changed obviously comparing with the TiO_2 NP photoelectrode. The top morphology SEM image of TiO_2 C/NP (12.5 wt.%) is shown in Fig. 2(a). There are minority of cavities formed among TiO_2 NPs in comparison with Fig. S1(a). The size of these cavities is around 350 nm, which is much bigger than pores observed in Fig. S1(a), indicating that the cavities are built by burning out carbonaceous microspheres. Another noticeable change is that the number of cavities increased as the weight ratio of carbonaceous microspheres was adjusted from 12.5 to 25 and 37.5 wt.%, as shown in Figs. 2(b) and 2(c). This variation demonstrates that the number of cavities can be easily tuned in the double-layered TiO_2 C/NP photoelectrode by adding different quantities of carbonaceous microspheres. Figure 2(d) exhibits the cross-section view of TiO_2 C/NP (25 wt.%). Clearly, a new TiO_2 NP layer embedded with cavities formed on the top of the dense TiO_2 NP layer. It can be discerned from Fig. 2(e) that these ~350 nm size of cavities distributed randomly across the top layer of TiO_2 C/NP, which is in agreement with Fig. 2(b).

The formation mechanism of TiO_2 cavities layer on top of TiO_2 NPs layer is presented in Fig. 3. As hard template, carbonaceous microspheres play important role in making cavities. During the heating process at 450 °C, carbonaceous microspheres in the mixture containing TiO_2 NPs and carbonaceous microspheres on the top of the TiO_2 NP layer were burned out gradually, leaving cavities surrounded by TiO_2 NPs. Therefore, the numbers of cavities in the top layer can be easily controlled just by varying the weight ratio of carbonaceous microspheres, forming different types of TiO_2 C/NP photoelectrodes. On the basis of the light scattering theory [31], these cavities may be possible to generate strong light-scattering effect in the double-layered TiO_2 C/NP photoelectrode.

Based on TiO_2 C/NP photoelectrodes, DSSCs have been assembled and their *J*–*V* performances have been also investigated. Figure 4 presents *J*–*V* curves of the DSSCs assembled with the TiO_2 NP photoelectrode and three types of TiO_2 C/NP photoelectrodes. Table 1 also lists the important photovoltaic parameters including short-circuit current density (J_{sc}), open circuit voltage (V_{oc}), fill factor (FF), and power conversion efficiency (PCE). The other two photoelectrodes including TiO_2 C/NP (6.25 wt.%) and TiO_2 C/NP (50 wt.%) have also been tested and their *J*–*V* curves are presented in Fig. S3 (see ESI). The results show that the photovoltaic performances of DSSCs based on such two TiO_2 C/NP photoelectrodes are lower than that of the DSSC based on any photoelectrodes of TiO_2 C/NP (12.5 wt.%), TiO_2 C/NP (25 wt.%), and TiO_2 C/NP (37.5 wt.%). Therefore, we focused on the investigation of the TiO_2 C/NP photoelectrode prepared separately with 12.5, 25, and 37.5 wt.% carbonaceous microspheres. The DSSC based on the TiO_2 NP photoelectrode shows the PCE of 4.57% with the J_{sc} of 10.73 mA·cm^{-2}, the V_{oc} of 0.71 V, and the FF of 0.60, while for the DSSC based on the TiO_2 NP photoelectrode on the top of which TiO_2 cavities formed, the photovoltaic performance improved significantly, especially for the J_{sc} and the PCE. For example, the J_{sc} of the DSSC based on TiO_2 C/NP (12.5 wt.%) increased to 15.20 mA·cm^{-2}, with the V_{oc} of 0.72 V and the FF of 0.55, producing the PCE of 6.02%. Moreover, the number

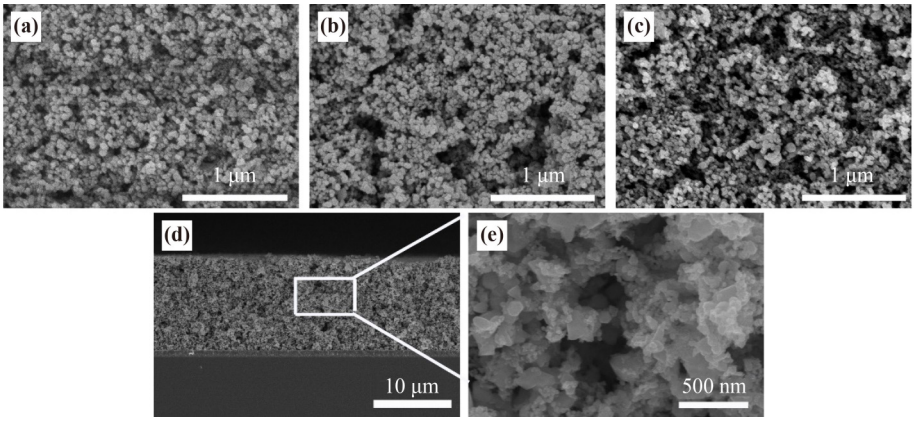

Fig. 2 (**a**)(**b**)(**c**) Top surface morphologies of TiO_2 C/NP photoelectrodes prepared by 12.5, 25, and 37.5 wt.% carbonaceous microspheres (from left to right). (**d**) The cross-section view of the TiO_2 C/NP photoelectrode. (**e**) Magnified SEM image of the selected local zone from panel (d).

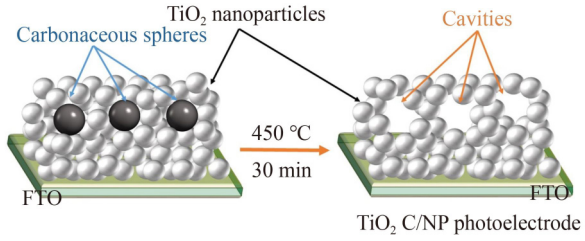

Fig. 3 The formation mechanism of the TiO_2 C/NP photoelectrode using carbonaceous microspheres as the hard template.

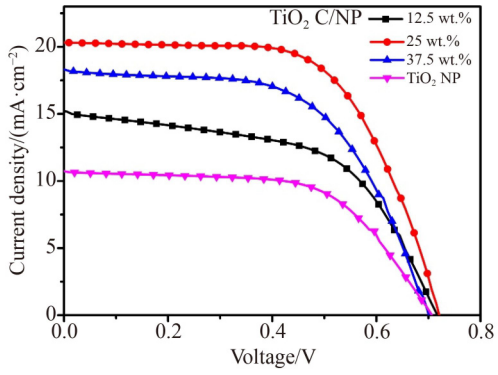

Fig. 4 *J–V* curves of DSSCs based on TiO_2 NP, TiO_2 C/NP (12.5 wt.%), TiO_2 C/NP (25 wt.%), and TiO_2 C/NP (37.5 wt.%).

Table 1 *J–V* parameters of DSSCs assembled with different photoelectrodes of TiO_2 NP and three types of TiO_2 C/NP

Photoelectrode	DSSC performance			
	J_{sc}/(mA·cm^{-2})	V_{oc}/V	FF	PCE/%
TiO_2 NP	10.73	0.71	0.60	4.57
TiO_2 C/NP (12.5 wt.%)	15.20	0.72	0.55	6.02
TiO_2 C/NP (25 wt.%)	20.35	0.72	0.62	9.08
TiO_2 C/NP (37.5 wt.%)	18.31	0.70	0.58	7.43

of cavities in TiO_2 C/NP also has influence on the photovoltaic performance. The DSSC based on TiO_2 C/NP (25 wt.%) shows the J_{sc} of 20.35 mA·cm^{-2}, the V_{oc} of 0.72V, the FF of 0.62, and the PCE of 9.08%, in which the J_{sc} and the PCE are the highest in the sample solar cells. However, a further increase of the cavity number in the TiO_2 C/NP photoelectrode reduced the DSSC performance. The TiO_2 C/NP (37.5 wt.%) produces the PCE of 7.43% with the J_{sc} of 18.31 mA·cm^{-2}, the V_{oc} of 0.70 V, and the FF of 0.58. On the basis of the *J–V* curve, it can be found that the great improvement of the J_{sc} is the most key factor that contributes to the increment of the PCE.

The only difference of these DSSCs is the cavities formed in the top layer of TiO_2 C/NP in comparison with the TiO_2 NP photoelectrode. Therefore, we infer that TiO_2 C/NP may combine advantages of TiO_2 NP and cavities together, resulting in the enhancement of the photovoltaic performance. Figure 5 sketches the configuration of the DSSC based on the TiO_2 C/NP photoelectrode. The TiO_2 C/NP may have two effects: (i) guarantee of almost the same dye adsorption comparing to TiO_2 NP, and (ii) stronger light-scattering effect caused by cavities.

Figure 6 provides N_2 adsorption–desorption curves of TiO_2 C/NP (25 wt.%), showing the specific surface area is 59.18 m^2·g^{-1} which is very close to that of TiO_2 NP as shown in Fig. S2 (see ESI). Both TiO_2 C/NP and TiO_2 NP photoelectrodes are built by P25, so the specific surface area changed slightly. This also proves that the formation of TiO_2 C/NP can continue to maintain the advantages of TiO_2 NPs in the dye adsorption.

It is well known that the light scattering of the TiO_2 photoelectrode is a crucial factor influencing the light harvesting efficiency (LHE) and then the PCE of DSSCs [31]. Figure 7(a) compares the DRS properties of TiO_2 NP

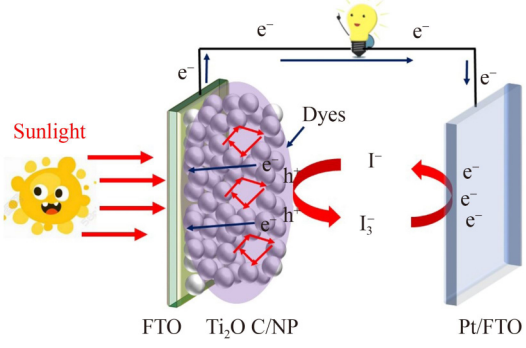

Fig. 5 Configuration of the DSSC based on the TiO_2 C/NP photoelectrode.

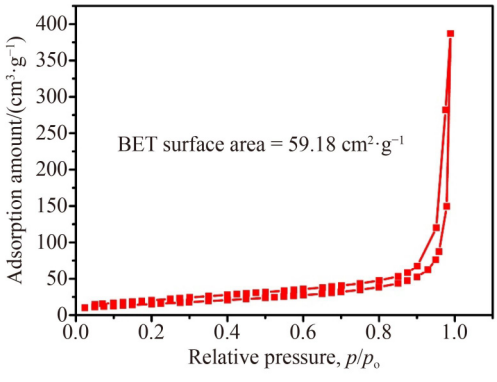

Fig. 6 N_2 adsorption–desorption curves of TiO_2 C/NP (25 wt.%).

and TiO_2 C/NP (25 wt.%). Obviously, TiO_2 C/NP has a higher reflectance than TiO_2 NP in the visible region, indicating a stronger light scattering. In the case of TiO_2 C/NP, the cavities in the size of ~350 nm is beneficial to generate stronger light scattering than TiO_2 NP because the cavity size is close to the visible-light wavelength [32]. A stronger light scattering can improve the LHE. Therefore, it is anticipatable that an increment of IPCE can be achieved with the DSSC based on TiO_2 C/NP. The relationship between IPCE and LHE is as follows [33]:

$$\mathrm{IPCE} = \mathrm{LHE} \times \Phi_{\mathrm{inj}} \times \eta_{\mathrm{cc}} \tag{1}$$

where Φ_{inj} and η_{cc} represent the charge injection efficiency and the charge collection efficiency, respectively. Figure 7 (b) illustrates the IPCE of DSSCs assembled with TiO_2 NP and TiO_2 C/NP (25 wt.%), demonstrating that TiO_2 C/NP contributes a higher IPCE. This result is in consistence with the J_{sc} in Fig. 4 which is expressed by Eq. (2) [34] as follows:

$$J_{\mathrm{sc}} = \int_{\lambda_1}^{\lambda_2} F(\lambda)\delta(\lambda)\mathrm{d}\lambda \tag{2}$$

where λ_1 and λ_2 denote the starting point and the ending point of the wavelength, respectively, $F(\lambda)$ represents the photon flux, and δ represent the IPCE. The TiO_2 C/NP (25 wt.%) photoelectrode generates stronger light scattering and boosts the LHE, improving the IPCE and the J_{sc}.

Although the existence of cavities on the top of TiO_2 NP layer plays an important role in promoting J_{sc}, the further increment of the cavity amount such as TiO_2 C/NP (37.5 wt.%) decreased the J_{sc} to 18.31 $\mathrm{mA \cdot cm^{-2}}$, which indicates that there may be an opposite effect between light scattering and charges recombination in the TiO_2 C/NP photoelectrode. Therefore, we speculate that more cavities in the TiO_2 C/NP photoelectrode may prolong the pathway of electrons, increasing the opportunities of charges recombination. In order to verify this speculation, the OCVD measurement results are shown in Fig. 8(a). Interestingly, the TiO_2 C/NP (25 wt.%) solar cell exhibits a faster V_{oc} decay rate than the DSSC based on TiO_2 NP and a slower decay rate than the DSSC based on TiO_2 C/NP (37.5 wt.%). The electron lifetime (τ_{n}) can be directly revealed by the slope of the V_{oc} decay curve according to Eq. (3) [35]:

$$\tau_{\mathrm{n}} = -\frac{k_{\mathrm{B}}T}{e}\left(\frac{\mathrm{d}V_{\mathrm{oc}}}{\mathrm{d}t}\right)^{-1} \tag{3}$$

where e, k_{B}, and T denote the electronic charge, the Bolzman constant, and the absolute temperature, respectively. The plot of τ_{n} versus V_{oc} are exhibited in Fig. 8(b), indicating that the order of electron lifetime from long to short is: TiO_2 NP, TiO_2 C/NP (25 wt.%), and TiO_2 C/NP (37.5 wt.%).

To further reveal the charges recombination dynamics, the EIS results of DSSCs assembled with TiO_2 NP, TiO_2 C/NP (25 wt.%), and TiO_2 C/NP (37.5 wt.%) are shown in Fig. 9. The spectra which are fitted by an equivalent circuit (inset of Fig. 9) shows two semi arcs. The small semi arc in high-frequency region is attributed to the recombination resistance at the counter electrode–electrolyte interface (R_{CE}) [36]. Another larger semi arc in low frequency represents the recombination resistance of photoexcited electrons at the TiO_2 photoelectrode–electrolyte interface (R_{rec}) [37]. The fitting results summarized from EIS data which are fitted by "Zview" software are listed in Table 2. A bigger second semi arc in low frequency indicates a higher recombination resistance

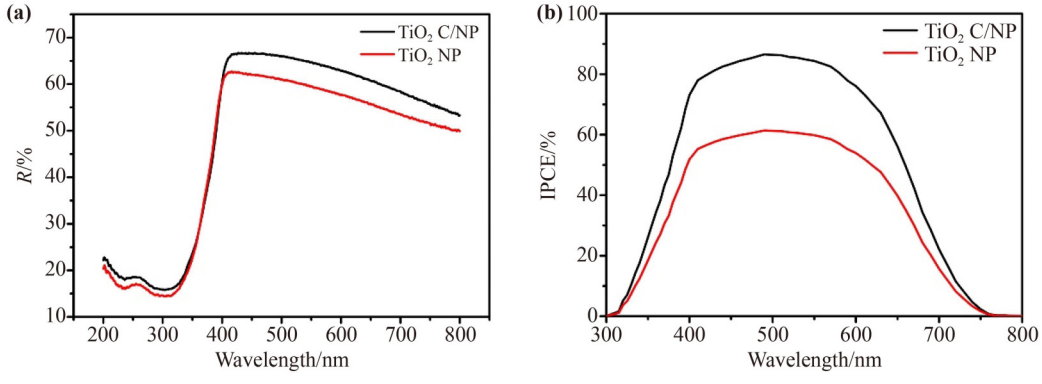

Fig. 7 (**a**) Diffused reflectance spectra of TiO_2 NP and TiO_2 C/NP (25 wt.%). (**b**) IPCE of DSSCs assembled with TiO_2 NP and TiO_2 C/NP (25 wt.%).

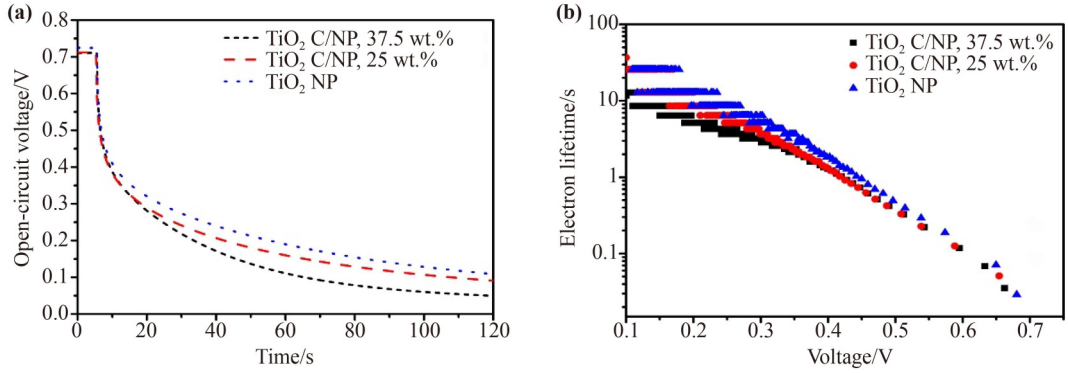

Fig. 8 (**a**) OCVD curves of DSSCs assembled with TiO_2 NP, TiO_2 C/NP (25 wt.%), and TiO_2 C/NP (37.5 wt.%). (**b**) Electron lifetime of DSSCs assembled with TiO_2 NP, TiO_2 C/NP (25 wt.%), and TiO_2 C/NP (37.5 wt.%).

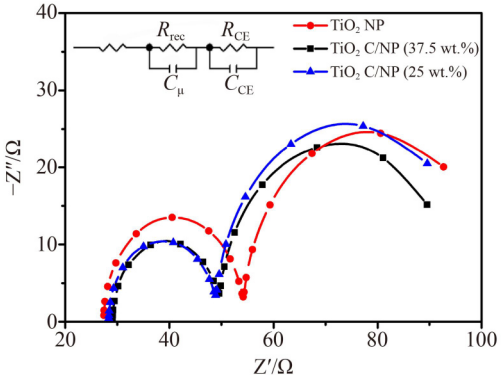

Fig. 9 EIS results of DSSCs assembled with TiO_2 NP, TiO_2 C/NP (25 wt.%), and TiO_2 C/NP (37.5 wt.%). The inset is equivalent circuit of DSSC.

Table 2 EIS fitting data of DSSCs assembled with different photoelectrodes of TiO_2 NP, TiO_2 C/NP (25 wt.%), and TiO_2 C/NP (37.5 wt.%)

Photoelectrode	EIS fitting results of the DSSC			
	R_{CE}/Ω	R_{rec}/Ω	C_μ/μF	τ_n/ms
TiO_2 NP	27	51	648	32
TiO_2 C/NP (25 wt.%)	21	49	602	30
TiO_2 C/NP (37.5 wt.%)	21	46	505	23

and a longer electron lifetime. The τ_n is determined by R_{rec} and C_μ as follows [38]:

$$\tau_n = R_{rec} \times C_\mu \quad (4)$$

Therefore, the electron lifetime values of DSSCs based on TiO_2 NP, TiO_2 C/NP (25 wt.%), and TiO_2 C/NP (37.5 wt.%) photoelectrodes are calculated to be 32, 30, and 23 ms, respectively. The trend of this result is consistent with that of OCVD, both of which verify that there is an opposite effect between light scattering and charges recombination in TiO_2 C/NP photoelectrodes. However, if the cavity amount is appropriately controlled in the TiO_2 C/NP photoelectrode, it is possible to make the strong light scattering play the key role in enhancing the J_{sc} significantly, leading to the improvement of the PCE, as revealed by the result of TiO_2 C/NP (25 wt.%).

4 Conclusions

Using carbonaceous microspheres as the template, TiO_2 cavities were built on the top of the TiO_2 NP layer, forming the double-layered TiO_2 C/NP photoelectrode for DSSCs. The cavity amount in the TiO_2 C/NP photoelectrode can be controlled by adjusting the weight ratio of the template. The TiO_2 C/NP has two positive effects on the increment of the J_{sc} when used in DSSCs, which include (i) guaranteeing almost the same dye adsorption comparing to TiO_2 NP, and (ii) enlarging light harvesting efficiency by generating strong light scattering through cavities. Although there is an opposite effect between the light scattering and the charge recombination in TiO_2 C/NP photoelectrodes, the light scattering can play a major role in enhancing the J_{sc} significantly by controlling the cavity amount appropriately in TiO_2 C/NP. Finally, based on the optimized TiO_2 C/NP (25 wt.%), the DSSC enables the PCE reach 9.08%, which is over 98% higher than the DSSC based on just the TiO_2 NP photoelectrode.

Acknowledgements This work was financially supported by the National Natural Science Foundation of China (Grant No. 51862007), the Western Youth Scholars Program of Chinese Academy of Sciences, and the Young Doctor Fund Project of Gansu Provincial Department of Education (Grant No. 2022QB-156).

Electronic supplementary information Supplementary materials can be found in the online version at https://doi.org/10.1007/s11706-023-0638-8.

References

[1] Devadiga D, Selvakumar M, Shetty P, et al. Recent progress in dye sensitized solar cell materials and photo-supercapacitors: a review. Journal of Power Sources, 2021, 493: 229698

[2] Ahmad M S, Pandey A K, Rahim N A. Advancements in the development of TiO_2 photoanodes and its fabrication methods for dye sensitized solar cell (DSSC) applications: a review. Renewable & Sustainable Energy Reviews, 2017, 77: 89–108

[3] Grätzel M. Photoelectrochemical cells. Nature, 2001, 414(6861): 338–344

[4] Yun S, Vlachopoulos N, Qurashi A, et al. Dye sensitized photoelectrolysis cells. Chemical Society Reviews, 2019, 48(14): 3705–3722

[5] Muñoz-García A B, Benesperi I, Boschloo G, et al. Dye-sensitized solar cells strike back. Chemical Society Reviews, 2021, 50(22): 12450–12550

[6] Ismael M. A review and recent advances in solar-to-hydrogen energy conversion based on photocatalytic water splitting over doped-TiO_2 nanoparticles. Solar Energy, 2020, 211: 522–546

[7] Daneshvar S, Saed A E, Sadrnezhaad S K. Hierarchical rutile/anatase TiO_2 nanorod/nanoflower thin film: synthesis and characterizations. Materials Science in Semiconductor Processing, 2019, 93: 252–259

[8] Bu C, Liu Y, Yu Z, et al. Highly transparent carbon counter electrode prepared via an *in situ* carbonization method for bifacial dye-sensitized solar cells. ACS Applied Materials & Interfaces, 2013, 5(15): 7432–7438

[9] Wang X, Zhao B, Kan W, et al. Review on low-cost counter electrode materials for dye-sensitized solar cells: effective strategy to improve photovoltaic performance. Advanced Materials Interfaces, 2022, 9(2): 2101229

[10] Song H, Pan Z, Rao H, et al. TiO_2 hierarchical nanowire-P25 particulate composite photoanodes in combination with N-doped mesoporous carbon/Ti counter electrodes for high performance quantum dot-sensitized solar cells. Solar Energy, 2019, 191: 459–467

[11] Gao Y, Nie W, Zhu Q, et al. The polarization effect in surface-plasmon-induced photocatalysis on Au/TiO_2 nanoparticles. Angewandte Chemie International Edition, 2020, 59(41): 18218–18223

[12] Marandi M, Farahani F A, Davoudi M. Fabrication of submicron/micron size cavities included TiO_2 photoelectrodes and optimization of light scattering to improve the photovoltaic performance of CdS quantum dot sensitized solar cells. Journal of Electroanalytical Chemistry, 2017, 799: 167–174

[13] Deepak T G, Anjusree G S, Thomas S, et al. A review on materials for light scattering in dye-sensitized solar cells. RSC Advances, 2014, 4(34): 17615–17638

[14] Huang F, Chen D, Zhang X L, et al. Dual-function scattering layer of submicrometer-sized mesoporous TiO_2 beads for high-efficiency dye-sensitized solar cells. Advanced Functional Materials, 2010, 20(8): 1301–1305

[15] Chen D, Huang F, Cheng Y B, et al. Mesoporous anatase TiO_2 beads with high surface areas and controllable pore sizes: a superior candidate for high-performance dye-sensitized solar cells. Advanced Materials, 2009, 21(21): 2206–2210

[16] Sauvage F, Chen D, Comte P, et al. Dye-sensitized solar cells employing a single film of mesoporous TiO_2 beads achieve power conversion efficiencies over 10%. ACS Nano, 2010, 4(8): 4420–4425

[17] Guo K, Li M, Fang X, et al. Improved properties of dye-sensitized solar cells by multifunctional scattering layer of yolk–shell-like TiO_2 microspheres. Journal of Power Sources, 2014, 264: 35–41

[18] Sheng J, Hu L, Li W, et al. Formation of single-crystalline rutile TiO_2 splitting microspheres for dye-sensitized solar cells. Solar Energy, 2011, 85(11): 2697–2703

[19] Huang Y, Wu H, Yu Q, et al. A single-layer TiO_2 film composed of mesoporous spheres for high-efficiency and stable dye-sensitized solar cells. ACS Sustainable Chemistry & Engineering, 2018, 6(3): 3411–3418

[20] Sun J, Guo H, Zhao L, et al. Co-sensitized efficient dye-sensitized solar cells with TiO_2 hollow sphere/nanoparticle double-layer film electrodes by Bi_2S_3 quantum dots and N719. International Journal of Electrochemical Science, 2017, 12: 7941–7955

[21] Hu H, Shen H, Cui C, et al. Preparation and photoelectrochemical properties of TiO_2 hollow spheres embedded TiO_2/CdS photoanodes for quantum-dot-sensitized solar cells. Journal of Alloys and Compounds, 2013, 560: 1–5

[22] Liu Y, Lan K, Bagabas A A, et al. Ordered macro/mesoporous TiO_2 hollow microspheres with highly crystalline thin shells for high-efficiency photoconversion. Small, 2016, 12(7): 860–867

[23] Zhu K, Neale N R, Miedaner A, et al. Enhanced charge-collection efficiencies and light scattering in dye-sensitized solar cells using oriented TiO_2 nanotubes arrays. Nano Letters, 2007, 7(1): 69–74

[24] Lee K S, Kwon J, Im J H, et al. Size-tunable, fast, and facile synthesis of titanium oxide nanotube powders for dye-sensitized solar cells. ACS Applied Materials & Interfaces, 2012, 4(8): 4164–4168

[25] Rui Y, Li Y, Zhang Q, et al. Size-tunable TiO_2 nanorod microspheres synthesised via a one-pot solvothermal method and used as the scattering layer for dye-sensitized solar cells.

Nanoscale, 2013, 5(24): 12574–12581

[26] Musavi Gharavi P S, Mohammadi M R. The improvement of light scattering of dye-sensitized solar cells aided by a new dandelion-like TiO_2 nanostructures. Solar Energy Materials and Solar Cells, 2015, 137: 113–123

[27] Yang G, Zhang J, Wang P, et al. Light scattering enhanced photoanodes for dye-sensitized solar cells prepared by carbon spheres/TiO_2 nanoparticle composites. Current Applied Physics, 2011, 11(3): 376–381

[28] Du X, Zhao L, He X, et al. TiO_2 hierarchical pores/nanorod arrays composite film as photoanode for quantum dot-sensitized solar cells. Journal of Energy Chemistry, 2019, 30: 1–7

[29] Ren H, Yu R, Wang J, et al. Multishelled TiO_2 hollow microspheres as anodes with superior reversible capacity for lithium ion batteries. Nano Letters, 2014, 14(11): 6679–6684

[30] Grätzel M. Solar energy conversion by dye-sensitized photovoltaic cells. Inorganic Chemistry, 2005, 44(20): 6841–6851

[31] Zhang Q, Chou T P, Russo B, et al. Polydisperse aggregates of ZnO nanocrystallites: a method for energy-conversion-efficiency enhancement in dye-sensitized solar cells. Advanced Functional Materials, 2008, 18(11): 1654–1660

[32] Huang F, Tang H, Wang Y, et al. Hierarchical ZnO microspheres photoelectrodes assembled with Zn chalcogenide passivation layer for high efficiency quantum dot sensitized solar cells. Journal of Power Sources, 2018, 401: 255–262

[33] Zhao H, Wu Q, Hou J, et al. Enhanced light harvesting and electron collection in quantum dot sensitized solar cells by TiO_2 passivation on ZnO nanorod arrays. Science China Materials, 2017, 60(3): 239–250

[34] Dang X, Qi J, Klug M T, et al. Tunable localized surface plasmon-enabled broadband light-harvesting enhancement for high-efficiency panchromatic dye-sensitized solar cells. Nano Letters, 2013, 13(2): 637–642

[35] Jiang D, Hao Y, Shen R, et al. Effective blockage of the interfacial recombination process at TiO_2 nanowire array electrodes in dye-sensitized solar cells. ACS Applied Materials & Interfaces, 2013, 5(22): 11906–11912

[36] Mora-Seró I, Giménez S, Fabregat-Santiago F, et al. Recombination in quantum dot sensitized solar cells. Accounts of Chemical Research, 2009, 42(11): 1848–1857

[37] Song H, Lin Y, Zhang Z, et al. Improving the efficiency of quantum dot sensitized solar cells beyond 15% via secondary deposition. Journal of the American Chemical Society, 2021, 143(12): 4790–4800

[38] Wang W, Du J, Ren Z, et al. Improving loading amount and performance of quantum dot-sensitized solar cells through metal salt solutions treatment on photoanode. ACS Applied Materials & Interfaces, 2016, 8(45): 31006–31015